



Original Article

Injectable phase-separated tetra-armed poly(ethylene glycol) hydrogel scaffold allows sustained release of growth factors to enhance the repair of critical bone defects



Shant Nepal ^a, Jinyan Si ^a, Shohei Ishikawa ^a, Masaki Nishikawa ^b, Yasuyuki Sakai ^{a,b}, Aya M. Akimoto ^c, Hiroyuki Okada ^{d,e}, Shinsuke Ohba ^f, Ung-il Chung ^{a,d}, Takamasa Sakai ^{a,**}, Hironori Hojo ^{a,d,*}

^a Department of Bioengineering, Graduate School of Engineering, The University of Tokyo, Tokyo 113-8656, Japan

^b Department of Chemical Systems Engineering, Graduate School of Engineering, The University of Tokyo, Tokyo 113-8656, Japan

^c Department of Materials Engineering, School of Engineering, The University of Tokyo, Tokyo 113-8656, Japan

^d Center for Disease Biology and Integrative Medicine, Graduate School of Medicine, The University of Tokyo, Tokyo 113-8655, Japan

^e Department of Orthopaedic Surgery, Graduate School of Medicine, The University of Tokyo, Tokyo 113-8655, Japan

^f Department of Tissue and Developmental Biology, Graduate School of Dentistry, Osaka University, Osaka 565-0871, Japan

ARTICLE INFO

Article history:

Received 29 September 2023

Received in revised form

13 November 2023

Accepted 16 November 2023

Keywords:

Polyethylene glycol

Injectable hydrogel

Gel-gel phase separation

Growth factors

Sustained release

Bone regeneration

ABSTRACT

With the rising prevalence of bone-related injuries, it is crucial to improve treatments for fractures and defects. Tissue engineering offers a promising solution in the form of injectable hydrogel scaffolds that can sustain the release of growth factors like bone morphogenetic protein-2 (BMP-2) for bone repair. Recently, we discovered that tetra-PEG hydrogels (Tetra gels) undergo gel-gel phase separation (GGPS) at low polymer content, resulting in hydrophobicity and tissue affinity. In this work, we examined the potential of a newer class of gel, the oligo-tetra-PEG gel (Oligo gel), as a growth factor-releasing scaffold. We investigated the extent of GGPS occurring in the two gels and assessed their ability to sustain BMP-2 release and osteogenic potential in a mouse calvarial defect model. The Oligo gel underwent a greater degree of GGPS than the Tetra gel, exhibiting higher turbidity, hydrophobicity, and pore formation. The Oligo gel demonstrated sustained protein or growth factor release over a 21-day period from protein release kinetics and osteogenic cell differentiation studies. Finally, BMP-2-loaded Oligo gels achieved complete regeneration of critical-sized calvarial defects within 28 days, significantly outperforming Tetra gels. The easy formulation, injectability, and capacity for sustained release makes the Oligo gel a promising candidate therapeutic biomaterial.

© 2023, The Japanese Society for Regenerative Medicine. Production and hosting by Elsevier B.V. This is an open access article under the CC BY-NC-ND license (<http://creativecommons.org/licenses/by-nc-nd/4.0/>).

1. Introduction

As the global aging population steadily rises, the frequency of bone injuries, such as fractures and bone defects, is also increasing. In 2019, 178 million new fractures and 455 million cases of acute or

long-term symptoms associated with fractures were reported [1]. Additionally, according to statistics from 2021, osteoporosis, a degenerative bone disease, affects approximately 18.3 % of the global population, or 1 in every 5 individuals [2]. These present bone injuries as a significant public health concern.

Treatment of non-union fractures and critical-sized bone defects remains challenging, even in current clinical practices. Autologous grafts, widely considered the clinical gold standard for repairing defects, are limited by donor source availability, and require highly invasive surgical procedures that result in donor site morbidity, infection and pain [3–5]. It has long-term adverse effects that include high failure rates and complications [4]. To overcome these challenges, tissue engineering has emerged as a promising

* Corresponding author. The University of Tokyo, 7-3-1 Hongo, Bunkyo-ku, Tokyo, 113-8656, Japan.

** Corresponding author.

E-mail addresses: t-sakai@g.ecc.u-tokyo.ac.jp (T. Sakai), hojo@g.ecc.u-tokyo.ac.jp (H. Hojo).

Peer review under responsibility of the Japanese Society for Regenerative Medicine.

approach, potentially in the form of biomaterial scaffolds that can control the delivery of growth factors and facilitate bone regeneration.

Synthetic polymer scaffolds have become an attractive option owing to their biocompatibility, defined chemical formulations for easy reproducibility, and precise mechanical tunability [6,7]. Hydrogels are particularly appealing for tissue engineering and drug delivery. Hydrogels are composed of a three-dimensional (3D) network of hydrophilic polymer chains that can mimic the native extracellular matrix (ECM) of bone [8]. The structure and permeability of the network can allow for controlled release of growth factors or bioactive molecules [9,10].

In 2008, we developed and introduced the tetra-armed poly (ethylene glycol) (PEG) hydrogel, or Tetra gel. This synthetic hydrogel is formed by crosslinking mutually reactive symmetrical tetrahedron-like PEG macromonomers and possesses several desirable qualities including biocompatibility, ease of fabrication, *in situ* gelation ability, and excellent mechanical properties [11,12]. However, similar to most conventional hydrogels, when used *in vivo*, these gels tend to swell, compromising their mechanical stability [13].

In 2017, we developed a novel type of tetra-PEG hydrogel, known as the oligo-tetra-PEG hydrogel or Oligo gel [14]. It was chemically identical to the conventional Tetra gel, but its gelation process differed. Tetra gels are formed in a conventional one-step process crosslinking mutually reactive tetra-PEG precursors via Michael addition [11]. Oligo gels are formed in a two-step process, where mutually reactive tetra-PEG precursors are crosslinked to form highly branched clusters in the sol region close to the sol-gel transition line, and then co-crosslinked to form gels. This two-step process resulted in a novel gel with improved mechanical properties, such as extremely low swelling, and fast, efficient *in situ* gelation at an ultralow polymer content, which may be advantageous for various clinical biomedical applications [14].

More recently, we discovered that at low polymer content, Tetra gels undergo percolation-induced gel-gel phase separation (GGPS) in aqueous conditions, leading to the formation of a hydrophobic filamentous network structure that promotes cell-gel interactions [15]. Such interactions are not possible in conventional synthetic bioinert PEG gels. Consequently, Tetra gels unexpectedly exhibited hydrophobicity and affinity for living tissues [15]. However, the extent to which GGPS occurs in the Tetra and Oligo gels remains unclear. Thus, we hypothesized that comparing these two types of gels would provide valuable insights into the mechanisms of GGPS and biological properties of the gels, which may be relevant to tissue engineering research.

In this study, we examined GGPS in Oligo gels and found that it occurs at a degree significantly stronger than that in conventional Tetra gels at low polymer content.

2. Materials and methods

2.1. Preparation of Tetra and Oligo gels

Tetra-armed polyethylene glycol ($M_w = 10 \text{ kg mol}^{-1}$) functionalized with sulfhydryl (tetra-PEG-SH, Lot No. P2205070130902-B) and maleimide (tetra-PEG-MA, Lot No. P2211070190901-B) were purchased from SINOPEG Biotech Co., Ltd. (Fujian, China). The substitutions of SH and MA were 98.3 % and 96.4 %, respectively (determined by $^1\text{H NMR}$).

For conventional Tetra gels, appropriate amounts of tetra-PEG-SH and tetra-PEG-MA were dissolved in citrate-phosphate buffer (CPB) (pH 5.0, salt concentration, 50 mM) to obtain 10 g l^{-1} solutions each. These pre-gel solutions were mixed in equal amounts. The resulting 10 g l^{-1} gels were left to stand for 24 h.

For Oligo gels, appropriate amounts of tetra-PEG-SH and tetra-PEG-MA were dissolved in CPB (pH 5.0, salt concentration, 50 mM) to obtain 20 g l^{-1} solutions each. In one vial, tetra-PEG-SH and tetra-PEG-MA solutions were mixed at a ratio of 78:22. In another vial, tetra-PEG-SH and tetra-PEG-MA solutions were mixed at a ratio of 22:78. The two resulting solutions were left to stand for 24 h before diluting with CPB to a concentration of 10 g l^{-1} . These pre-gel solutions were mixed in equal amounts. The resulting 10 g l^{-1} gels were then left to stand for 24 h.

For *in vitro* and *in vivo* studies, pre-gel solutions were sterilized by filtering through a 28 mm-diameter, 0.2 μm -pore size surfactant-free cellulose acetate (SFCA) membrane sterile syringe filter (431219, Corning Inc.).

2.2. UV-vis spectra of gels

Tetra and Oligo gels were prepared in plastic cells with an optical length of 10 mm. The transmittance at $\lambda = 400 \text{ nm}$ was measured at room temperature using a UV-vis spectrophotometer (V-670, JASCO Corp.). The turbidity was estimated by normalizing absorbance with polymer concentration (g l^{-1}) and optical length (m).

2.3. Hydrophobic microparticle adsorption to gels

Tetra and Oligo gels (15 mm-diameter) were immersed in a 0.1 % w/v solution of Fluoresbrite® YG Carboxylate Microspheres (10 μm -diameter, Polysciences Inc.) in water for 24 h at room temperature. Images were obtained using an LSM 800 confocal laser microscope (Zeiss) and the number of particles were quantified using ImageJ.

2.4. Contact angle of gels

The contact angle of Tetra and Oligo gels (7 mm-diameter, 3 mm height) was evaluated. Gels were first immersed in water for 24 h at room temperature. Gels were then placed on a glass slide and set on a contact angle meter (DMS-401, Kyowa Interface Science Co., Ltd.). 1 μl of water was gently dropped onto the gel surface, and the contact angle measurement and image were obtained using the FAMES contact angle measurement software (Kyowa Interface Science Co., Ltd.).

2.5. Scanning electron microscopy

Gel surface morphological images were obtained using a TM3030 scanning electron microscope (Hitachi) under EDX observation conditions. Tetra and Oligo gels (15 mm-diameter) were immersed in water for 1–2 h before imaging. The microscope was capable of imaging gels in the wet state.

2.6. Protein release kinetics

Tetra and Oligo pre-gel solutions were loaded with fluorescein isothiocyanate-labeled bovine serum albumin (BSA) (FITC-BSA) (A23015, Thermo Fisher Scientific) or Protein A (FITC-Protein A) (ab7455, Abcam) at a concentration of 100 $\mu\text{g/ml}$ and then mixed to form gels (200 μl) in 12-well-size transwell Falcon® inserts that have a 1.0 μm membrane pore size (353103, Corning Inc.). We chose a loading concentration of 100 $\mu\text{g/ml}$ FITC-BSA in the gel based on previous studies [16,17]. We also employed the same concentration when loading FITC-Protein A for consistency. Transwell gel inserts were then placed in wells containing 1 ml phosphate buffered saline (PBS) (045-29795, FUJIFILM Wako) in a 12-well plate. At predetermined time points, the transwell gel inserts were removed and placed in fresh PBS. Fluorescence values of the released

samples at each time point were retrieved using an AD 200 plate reader (Beckman Coulter). Concentrations were interpolated using a prepared standard curve. Cumulative release profiles (%) were obtained by summing the mass eluted at each time point and normalizing it to the initial dose.

2.7. *In vitro* cell culture and osteoblast differentiation assay

MC3T3-E1 cells were obtained from the Riken Cell Bank (Tsukuba, Japan) and maintained in alpha Modified Eagle Minimum Essential Medium (MEM α) (11900-073, Thermo Fisher Scientific) supplemented with 10 % fetal bovine serum (FBS) (Lot. M30-2683268-1, Equitech-Bio) and 1 % penicillin/streptomycin (P4333, Sigma-Aldrich). For osteogenic culture, cells were cultured in osteogenic medium consisting of high glucose Dulbecco's Modified Eagle's Medium (D-MEM) (043-30085, FUJIFILM Wako) supplemented with 10 % FBS, 1 % penicillin/streptomycin, 50 μ g/ml ascorbic acid (012-04802, FUJIFILM Wako), 10 mM β -glycerophosphate (G9422-100G, Sigma-Aldrich), and 0.01 μ M dexamethasone (041-18861, FUJIFILM Wako).

For alkaline phosphatase (ALP) staining, cells were fixed in 70 % ethanol and stained for 15 min with a solution containing 0.02 % naphthol AS-MX phosphate disodium salt (N5000-1G, Sigma-Aldrich) and 0.1 % fast blue BB (F3378-5G, Sigma-Aldrich).

2.8. RNA extraction and reverse transcription-quantitative polymerase chain reaction (RT-qPCR)

Total RNA was extracted using ISOGEN (311-02501, Nippon Gene) and an RNeasy Mini Kit (74106, Qiagen). The quality and quantity of RNA from each sample were evaluated using a NanoDrop® ND-1000 spectrophotometer (Thermo Fisher Scientific). Next, 1 μ g of total RNA was reverse transcribed into complementary DNA (cDNA) using a ReverTra Ace™ qPCR RT Master Mix with gDNA Remover Kit (FSQ-301, Toyobo Co., Ltd.). For PCR reaction, 2 μ l cDNA was used for each reaction with a FastStart Universal SYBR Green Master Kit (04913 850001, Roche). RT-qPCR was performed using the 7500 Fast Real-Time PCR System (Applied Biosystems). *Actb* was used as mouse endogenous controls for the $\Delta\Delta$ CT method to evaluate relative mRNA expression. The following primer sequences were used:

Mouse actin beta, *Actb*: forward 5'-AGATGTGGATCAGCAAGCAG-3' reverse 5'-GCGCAAGTTAGGTTTTGTCA-3'.

Mouse alkaline phosphatase, *Alpl*: forward 5'-GCTGATCATCC-CACGTTTT-3' reverse 5'-CTGGGCTGGTAGTTGTGT-3'.

Mouse runt-related transcription factor 2, *Runx2*: forward 5'-CCCAGCCACCTTACTACA-3' reverse 5'-TATG-GAGTGCTGCTGGTCTG-3'.

Mouse integrin binding sialoprotein, *Ibsp*: forward 5'-CAGAG-GAGGCAAGCGTCACT-3' reverse 5'-CTGTCTGGGTGCCAACACTG-3'.

Mouse bone gamma-carboxyglutamic acid-containing protein, *Bglap*: forward 5'-AAGCAGAGGGCAATAAGGT-3' reverse 5'-TTTGTAGCGGCTTCAAGC-3'.

2.9. Mouse calvarial critical defect model

All mouse experiments were performed according to a protocol approved by the Animal Care and Use Committee of The University of Tokyo.

Mouse calvarial defects were created using a protocol adapted from Samsonraj et al. [18].

Eight-week-old male C57BL/6J mice were purchased from the Jackson Laboratory. In preparation for surgery, mice were quickly incapacitated using 2 % isoflurane in O₂ in an anesthesia inhalation chamber. They were then administered with an intraperitoneal

injection of a double drug anesthetic cocktail consisting of 10 mg/ml ketamine (Daiichi Sankyo Co., Ltd.) and 1.6 mg/ml xylazine (Bayer HealthCare Pharmaceuticals Inc.) in a final dose volume of 100 μ l per 10 g body weight. Hair was removed from the region between the eyes and the posterior end of the skull by an electric shaver. A deep longitudinal skin incision was made on the scalp starting from the midsagittal area of the skull to just behind the eyes. The incised skin was then retracted using the thumb and forefinger to expose the calvarium. Using a 3 mm biopsy punch (BP-30F, Kai Medical), a 3 mm-diameter defect was created on the right parietal bone of the calvarium. While creating the defect, the exposed site was kept wet with a saline solution. The 3 mm diameter excised bone was removed, and the defect site was washed with saline to remove any debris. Tetra and Oligo pre-gel solutions loaded with 2 μ g of recombinant human bone morphogenetic protein-2 (rhBMP-2) (7510050, INFUSE™ Bone Graft, Medtronic) were then mixed (20 μ l total) and injected onto the defect site. We chose a rhBMP-2 dose of 2 μ g per 20 g mouse body weight as it falls in the lower end of the clinically relevant dose range of 0.1–0.5 mg BMP-2 per kg body weight [19,20]. Once gelation was reached, the skin was closed using a nylon suture (B11-60N2, ELP®). A warm heating pad was used to maintain body temperatures of the mice throughout the procedures.

The mice were euthanized at 42 days post-operation. Calvaria tissues were harvested, fixed in cold 4 % paraformaldehyde in PBS (163-20145, FUJIFILM Wako) for 24 h, and stored in PBS until further use.

2.10. Micro-CT analysis

In vivo live micro-computed tomography (CT) scans of the calvarial defects were conducted at 1-, 14-, 28-, and 42-days post-operation using R_mCT2-FX (Rigaku) under the following conditions: 90 kV, 160 μ A, 24 FOV, and 17 sec. 3D reconstruction was performed using the manufacturer's software referring to recommendations by the American Society of Bone and Mineral Research (ASBMR) [21].

For assessing bone volume (BV) and bone mineral content (BMC), and visualizing bone density, micro-CT scans of harvested calvaria tissues were conducted using a SMX-90CT-SV (Shimadzu) under the following conditions: 90 kV and 160 μ A. TRI/3D-BON software (Ratoc System Engineering) was used for quantitative analysis.

2.11. Histological preparation and analysis

Calvarial tissue samples were decalcified with 0.5 M ethylenediaminetetraacetic acid (EDTA) in PBS at 4 °C for at least 5 days. Before preparing frozen blocks, the samples were incubated in 30 % sucrose in PBS at 4 °C overnight. Samples were then embedded in O.C.T. Compound (4583, Sakura Finetek™ Japan) and frozen at –100 °C.

12 μ m frozen sections were sliced using a CM3050IV cryotome (LEICA) onto slides (SCRE-01, Matusnami) and air-dried at room temperature before staining. Hematoxylin and eosin (H&E) and Masson's trichrome staining were performed for morphological studies. Immunohistochemistry was performed to visualize RUNX2 (ab192256, Abcam) and SP7 (ab22552, Abcam) by fluorescence with an Alexa 546 anti-rabbit IgG antibody (A-11035, Invitrogen). The dilution ratios for each antibody were 1:1000, 1:1000, and 1:500. Brightfield and fluorescence images were captured using a BZ-X700 fluorescence microscope (Keyence).

2.12. Statistical analysis

For the turbidity and hydrophobicity studies, three replicates were prepared for each gel. The *in vitro* protein release kinetics and

cell differentiation studies used three biological replicates for each sample group. Three technical replicates were prepared for RT-qPCR analysis. For the *in vivo* study, 3–4 mice were used per treatment group. Statistical analyses were performed using GraphPad Prism 9. Values are expressed as mean \pm standard deviation (SD). Other than the turbidity and hydrophobicity studies in which statistical significance was determined using Student's *t*-test, statistical significance was determined using two-way Analysis of Variance (ANOVA) followed by either Bonferroni's or Tukey's multiple comparisons test. Statistical significance was set at $P < 0.05$. *P*-values are denoted by asterisks in all figures.

3. Results

3.1. Assessment of gel-gel phase separation in Tetra and Oligo gels at low polymer content

To assess the degree of GGPS in the Tetra and Oligo gels, we first investigated the turbidity of the gels. Both gels were prepared as depicted in the schematic (Fig. 1a) with a PEG concentration of 10 g l^{-1} , and turbidity measurements were conducted 24 h post-gelation. We found the Oligo gel to be significantly more turbid, appearing much cloudier and measuring almost 5-fold higher than the Tetra gel (Fig. 1b).

Next, we examined the hydrophobicity of both gels. First, we immersed them in a solution of hydrophobic fluorescent microparticles. The Oligo gel adsorbed significantly more particles, almost 4-fold higher, to its surface than the Tetra gel (Fig. 1c). Then, we evaluated the contact angle of both gels by dropping a water droplet onto their surfaces. The Oligo gel had a significantly higher contact angle of 67° , in contrast to the Tetra gel's 52° (Fig. 1d). Both findings collectively suggest the Oligo gel has a higher degree of hydrophobicity.

Additionally, we employed SEM imaging to visualize the morphological differences between the gels within 1–2 h of water immersion. The surface of the Tetra gel generally appeared homogenous with small crater-like formations scattered throughout; the surface of the Oligo gel appeared heterogeneous with filamentous and pore structures of various sizes (Fig. 1e). Furthermore, in the areas of the Oligo gel without pore structures, we observed a swirling phenomenon, which possibly indicated the initiation of pore formation (Fig. 1e).

3.2. Characterizing release kinetics using growth factor-loaded Tetra and Oligo gels

Hydrophobic surfaces are known to have high protein binding affinity [22]. Thus, we theorized that the hydrophobicity of the Oligo gel would allow proteins or growth factors to bind more firmly to the gel and consequently sustain their release. To investigate growth factor release behavior from the Tetra and Oligo gels, we performed release kinetics studies using gels loaded with fluorescein isothiocyanate-labeled bovine serum albumin (FITC-BSA), a protein commonly used for such studies, or Protein A (FITC-Protein A), a protein that has previously been used as a model for BMP-2 [23–25]. Gels were formed by mixing pre-gel solutions loaded with FITC-BSA or FITC-Protein A into transwell inserts. Transwell inserts containing the FITC-loaded gels were placed in PBS, which was collected at various times (Fig. 2a). Cumulative release curves were constructed for both gels until approximately 100 % release was achieved.

We found that the Oligo gel sustained the release of FITC-BSA for a longer period than the Tetra gel (Fig. 2b, left panel). In the first 7 days, the Tetra gel released approximately 80 % of the FITC-BSA while the Oligo gel released approximately 60 % (Fig. 2b, right panel). By day 12, the Tetra gel reached around 100 % release.

Ultimately, it was not until day 17 that the Oligo gel reached almost 100 % release. The release of FITC-Protein A from the gels also followed a similar trend, albeit at a slightly faster rate (Fig. 2c). This is likely due to the size of FITC-Protein A being smaller ($\sim 40 \text{ kDa}$) than FITC-BSA ($\sim 66 \text{ kDa}$). These findings suggest that the high hydrophobicity obtained by the Oligo gel, as a result of the greater degree of GGPS, allowed it to sustain growth factor release.

3.3. *In vitro* osteogenic induction by rhBMP-2-loaded Tetra and Oligo gels

To further confirm the growth factor release behaviors from the Tetra and Oligo gels, we loaded the gels with recombinant human bone morphogenetic protein-2 (rhBMP-2), a potent bone growth factor [26], and examined their ability to induce osteoblast differentiation in MC3T3-E1 cells, a mouse pre-osteoblast cell line. Similar to the release kinetics study shown in Fig. 2, gels were formed by mixing pre-gel solutions loaded with a $2\text{-}\mu\text{g}$ dose of rhBMP-2 in transwell inserts. MC3T3-E1 cells were cultured with the gels, and the gels were transferred onto freshly prepared cells every 7 days (Fig. 3a).

Alkaline phosphatase (ALP) staining, a marker of osteogenesis [27], suggested the Tetra gels released rhBMP-2 at a much faster rate, as evidenced by a more drastic decrease in staining intensity with each new batch of cells. In contrast, the Oligo gels exhibited a steady decline in staining intensity, indicating a slow, sustained release of rhBMP-2 (Fig. 3b). Relative *Alpl* expression was consistent with the ALP staining. Comparing both gels, Tetra gels showed significantly higher expression on day 7, whereas the Oligo gels showed significantly higher expression on days 14 and 21 (Fig. 3b). Relative mRNA expressions of other osteoblast markers, such as *Runx2*, *Ibsp*, and *Bglap* also followed a similar trend. On days 7 and 14, both gels induced osteoblast differentiation as all tested markers were significantly upregulated compared to the control (Fig. 3b). However, on day 21, only the Oligo gels showed significant upregulation of all tested markers compared to the control, whereas the Tetra gels showed upregulation of only *Alpl* and *Runx2*, indicating that only early osteogenesis was induced (Fig. 3b). This further confirmed that over a 21-day period, the Oligo gels sustained the release of rhBMP-2 and successfully induced osteoblast differentiation in three different batches of cells. Overall, the osteogenic induction by both gels mirrored the release behavior observed in the release kinetics study (Fig. 2b and c, right panels).

3.4. *In vivo* cranial bone regeneration by rhBMP-2-loaded Tetra and Oligo gels

To evaluate bone regeneration, we used a mouse calvarial critical defect model due to its relatively easy surgical procedure, good standardization, and easier evaluation of biomaterials compared to long bone defect models [28,29]. We created 3 mm-diameter critical-sized defects in the calvariae of 8-week-old mice [4,5]. Tetra and Oligo gels were formed *in situ* by mixing pre-gel solutions with and without a $2\text{-}\mu\text{g}$ dose of rhBMP-2 per 20 g mouse body weight and injecting them onto the defect sites. Defects that were left untreated were used as a negative control.

In vivo 3D micro-CT analysis revealed that Tetra and Oligo gels without rhBMP-2 did not facilitate bone regeneration apart from minor healing along the defect edges after 42 days compared to the negative control (Fig. 4a & Supplementary Fig. 1). Oligo-rhBMP-2 gels showed significantly greater bone regeneration after 14 days compared to Tetra-rhBMP-2 gels. By 28 days post-operation, it was clear Oligo-rhBMP-2 gels performed significantly greater than Tetra-rhBMP-2 gels, completely regenerating new bone within the defect site (Fig. 4a and b). This observation was supported by

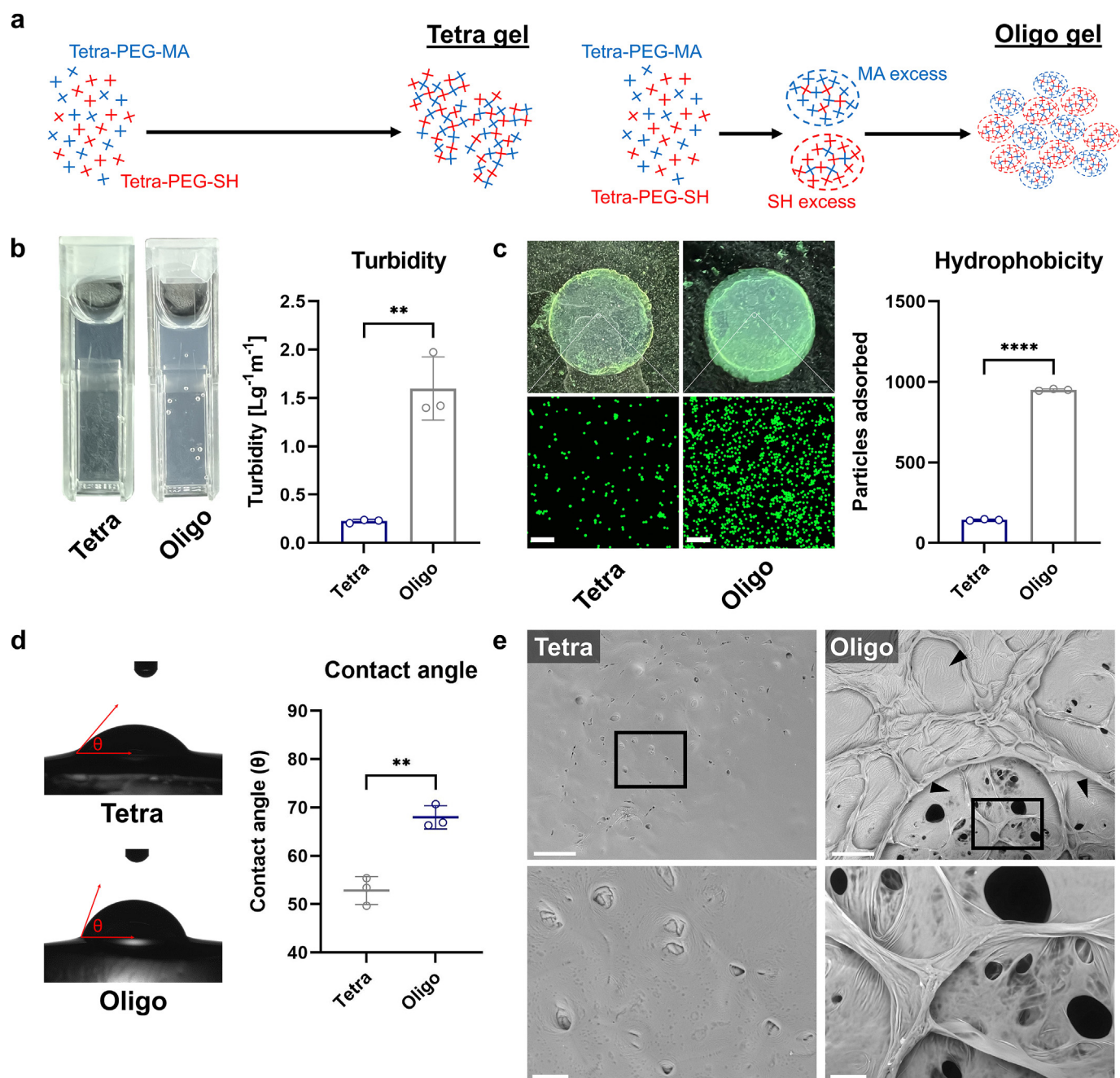


Fig. 1. Assessment and comparison of low concentration conventional tetra-armed PEG (Tetra) and oligo tetra-armed PEG (Oligo) hydrogels. (a) Schematic depicting the gelation process of Tetra and Oligo gels. (b) Turbidity measured using UV–Visible spectrophotometer. Data presented as mean \pm SD, $n = 3$. Statistical analysis performed using student's t-test. P-value ** <0.002 . (c) Adsorption of fluorescent hydrophobic microparticles to the hydrogel surface. Top row images are a whole view of the gels. Bottom row images are a magnified view. Scale bars, 100 μm . Data presented as mean \pm SD, $n = 3$. Statistical analysis performed using student's t-test. P-value **** <0.0001 . (d) Contact angles of the Tetra and Oligo gels at the point after their surface makes contact with the water droplet. Red arrows denote the angle measured. Data presented as mean \pm SD, $n = 3$. Statistical analysis performed using student's t-test. P-value ** <0.005 . (e) SEM images of the surfaces of the Tetra and Oligo gels. Left images are a wide view. Arrowheads and rectangles denote the swirling phenomenon and the location of magnified images, respectively. Scale bars, 250 μm . Right images are a magnified view. Scale bars, 50 μm .

quantitative analyses based on 3D micro-CT images. Oligo-rhBMP-2 gel-treated defects showed significantly higher bone volume (BV) and bone mineral content (BMC) than Tetra-rhBMP-2 gel-treated defects (Fig. 4c).

Histological analyses were performed to evaluate the regenerated bone within the defect site. H&E staining of representative day 42 sections revealed no substantial inflammation or foreign-body reactions in any samples from all gel groups, even in areas containing gel remnants (Fig. 5a & Supplementary Fig. 2). When

comparing both rhBMP-2-loaded gel groups, it was obvious only the Oligo-rhBMP-2 gel fully regenerated and bridged the defect with new bone (Fig. 5a). A closer examination of the new bone in the Tetra-rhBMP-2 gel group revealed a composition of mostly fibrous soft tissue and immature woven bone situated from the middle-to-top region, and a layer of mature lamellar bone at the bottom (Fig. 5b). This finding indicated that bone regeneration occurred in the bottom-to-top and edge-to-center directions. Masson's trichrome staining further confirmed this finding as the

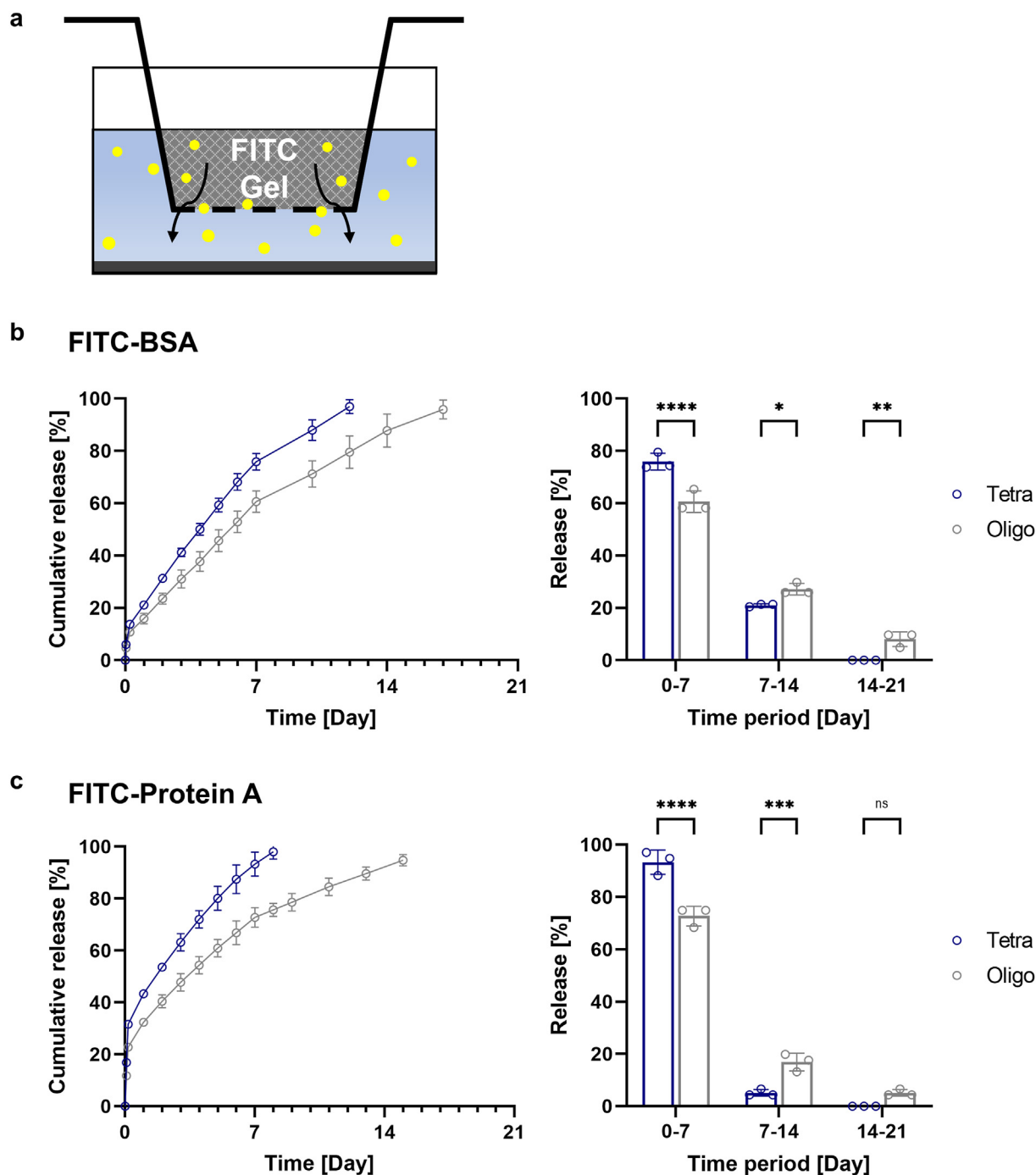


Fig. 2. Protein release characterization of Tetra and Oligo gels loaded with FITC-labeled protein. (a) Experiment schematic. Gels loaded with FITC-labeled protein (yellow particles in the schematic) were placed on transwells in PBS. At each time point, PBS was collected and measured for fluorescence intensity by a microplate reader. (b) Release profiles of FITC-BSA over a 21-day period. The left panel shows the cumulative release, and the right panel shows a comparison of percent release for each time period. Data presented as mean ± SD, n = 3. Statistical analysis performed using two-way ANOVA + Bonferroni's multiple comparisons test. P-value * <0.05, ** <0.01, **** <0.0001. (c) Release profiles of FITC-Protein A over a 21-day period. The left panel shows the cumulative release, and the right panel shows a comparison of percent release for each time period. Data presented as mean ± SD, n = 3. Statistical analysis performed using two-way ANOVA + Bonferroni's multiple comparisons test. P-value *** < 0.002, **** < 0.0001, ns – not significant.

bottom layer of the mature lamellar bone appeared red, indicating mineralization, while the middle-to-top region appeared blue, indicating the presence of collagen fibers or woven bone (Fig. 5b). By contrast, the new bone in the Oligo-rhBMP-2 gel group appeared more mature with more mineralized lamellar bone and bone marrow cavities structurally organized similar to that of intact healthy calvarial bone (Fig. 5b & Supplementary Fig. 3).

Additionally, immunostaining showed a stronger presence of RUNX2 and SP7, master regulators of osteoblast differentiation, in the Oligo-rhBMP-2 gel group than in the Tetra-rhBMP-2 gel group (Fig. 5c). Overall, these findings suggest that the Oligo gels sustained the release of rhBMP-2 which contributed to the complete regeneration of the calvarial bone defect with maturing bone, unlike the Tetra gels, which released rhBMP-2 at a much faster rate.

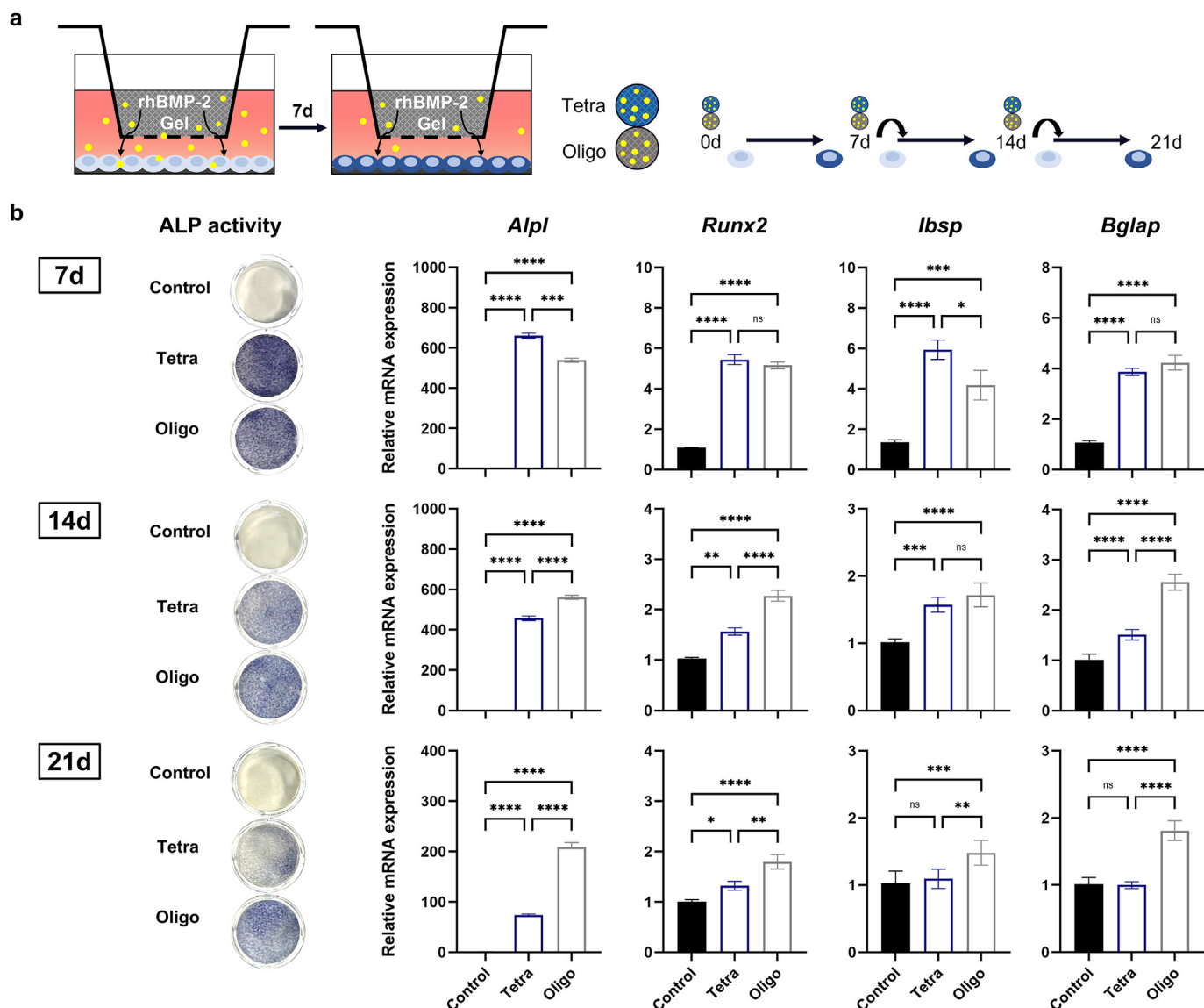


Fig. 3. Osteogenic induction on MC3T3-E1 cells by rhBMP-2-loaded Tetra and Oligo gels. (a) Experiment schematic. Gels loaded with rhBMP-2 (yellow particles in the schematic) were placed on transwells in osteogenic medium. Gels were transferred onto newly prepared cells after 7 days. (b) ALP activity and relative mRNA expression of *Alpl*, *Runx2*, *Ibsp*, and *Bglap* at 7d (top row), 14d (middle row), and 21d (bottom row). Data presented as mean \pm SD, $n = 3$. Statistical analysis performed using two-way ANOVA + Tukey's multiple comparisons test. P-value * <0.05, ** <0.005, *** <0.001, **** <0.0001, ns – not significant.

4. Discussion

This study compared the Oligo gel with the Tetra gel and yielded three key findings: (i) the Oligo gel exhibited significantly higher turbidity and hydrophobicity, indicating a greater degree of GGPS; (ii) it demonstrated sustained release of BSA, Protein A, and rhBMP-2 over a 21-day period; and (iii) it achieved complete regeneration of the mouse calvarial critical bone defect at a significantly faster rate.

In our previous study, we deduced that GGPS occurs in conventional Tetra gels with low PEG content when immersed in water, based on the significant increases in turbidity and the formation of a hydrophobic filamentous network structure within 1 week of immersion in water [15]. In this study, we found that even before water immersion, the Oligo gel exhibited significantly higher turbidity, possibly indicating the initiation of the GGPS process. Once immersed in water, SEM imaging revealed that the Oligo gel developed a similar network structure within a remarkably shorter

timeframe of 1–2 h. Moreover, SEM uncovered two distinct features that were not previously observed: (i) the formation of pores and (ii) a swirling phenomenon in areas without pores within the filamentous network. We hypothesized that the swirling phenomenon could also be signifying the initiation of GGPS, eventually leading to pore formation.

Growth factors play a vital role in signaling specific cellular responses [30]. Among the osteogenic growth factors, bone morphogenetic proteins (BMPs), such as BMP-2, are highly potent inducers of bone formation. BMP-2 has been utilized in the clinical treatment of non-union fractures, with typical doses ranging from 0.1–0.5 mg BMP-2 per kg body weight [19,20,31]. However, their short half-life, ranging from 7 to 16 min in circulation, and rapid clearance often necessitate supraphysiological doses of rhBMP-2 [32,33]. This can lead to adverse effects, including unwanted ectopic bone formation, resorption of native bone, and soft tissue inflammation [33]. To overcome these challenges, biomaterial scaffold-based delivery strategies offer a promising solution by

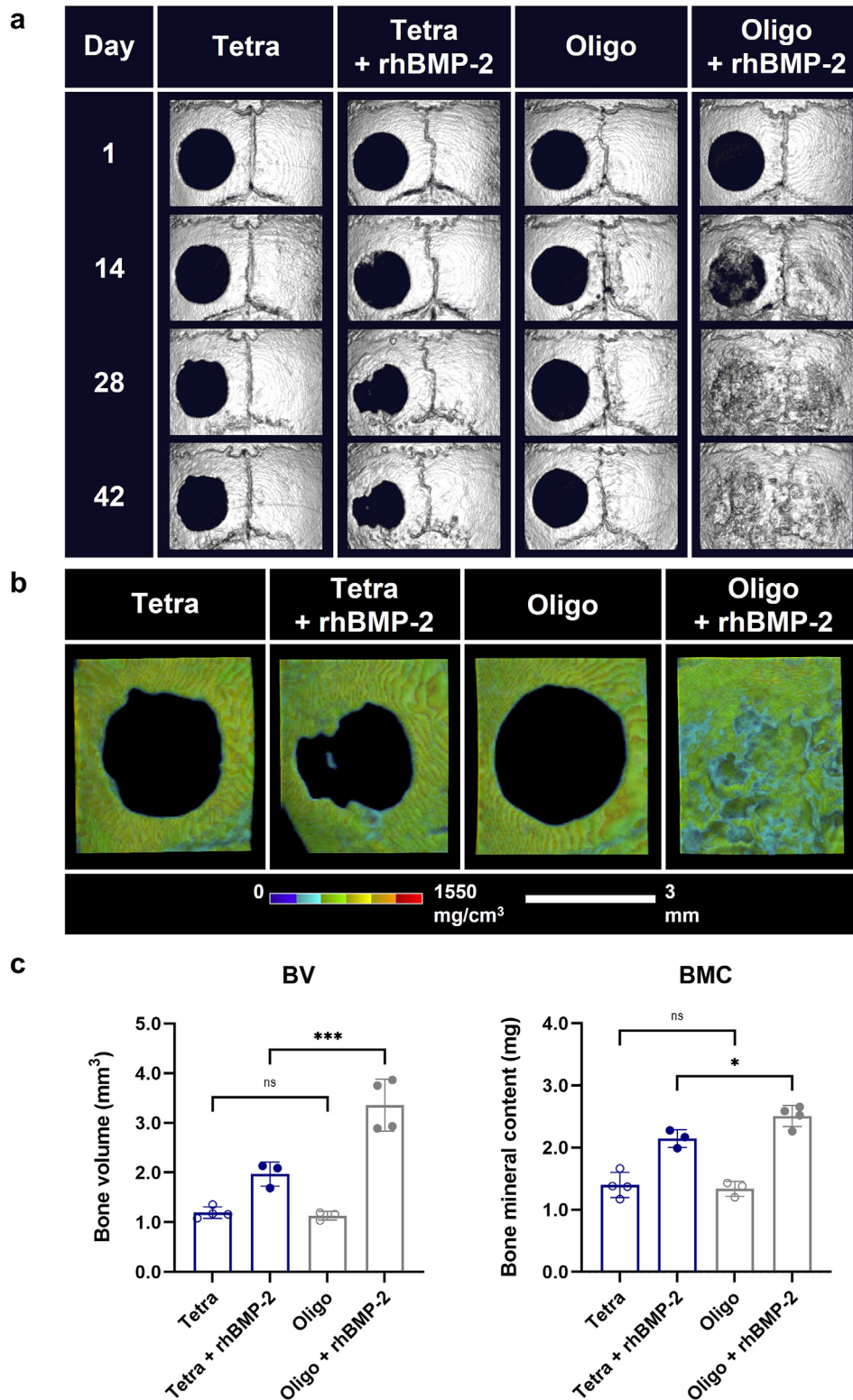


Fig. 4. Comparison of bone regeneration between Tetra and Oligo gels loaded with and without rhBMP-2 in a 3 mm-diameter mouse calvarial critical defect model over a 42-day period. (a) *In vivo* micro-CT representative images of defects at 1-, 14-, 28-, and 42-days post-operation. (b) Visualization of bone density of the defect site and surrounding area at 42 days post-operation. The same trimming dimension and approximate imaging location is used across all samples. Scale bar, 3 mm. (b) Quantitative measurement of bone mineral content (mg) and bone volume (mm³) of the defect site and surrounding cortical bone regions at 42 days, as represented in (b). Data presented as mean ± SD, n = 3 or 4. Statistical analysis performed using two-way ANOVA + Tukey's multiple comparisons test. P-value * <0.05, *** <0.001, ns – not significant.

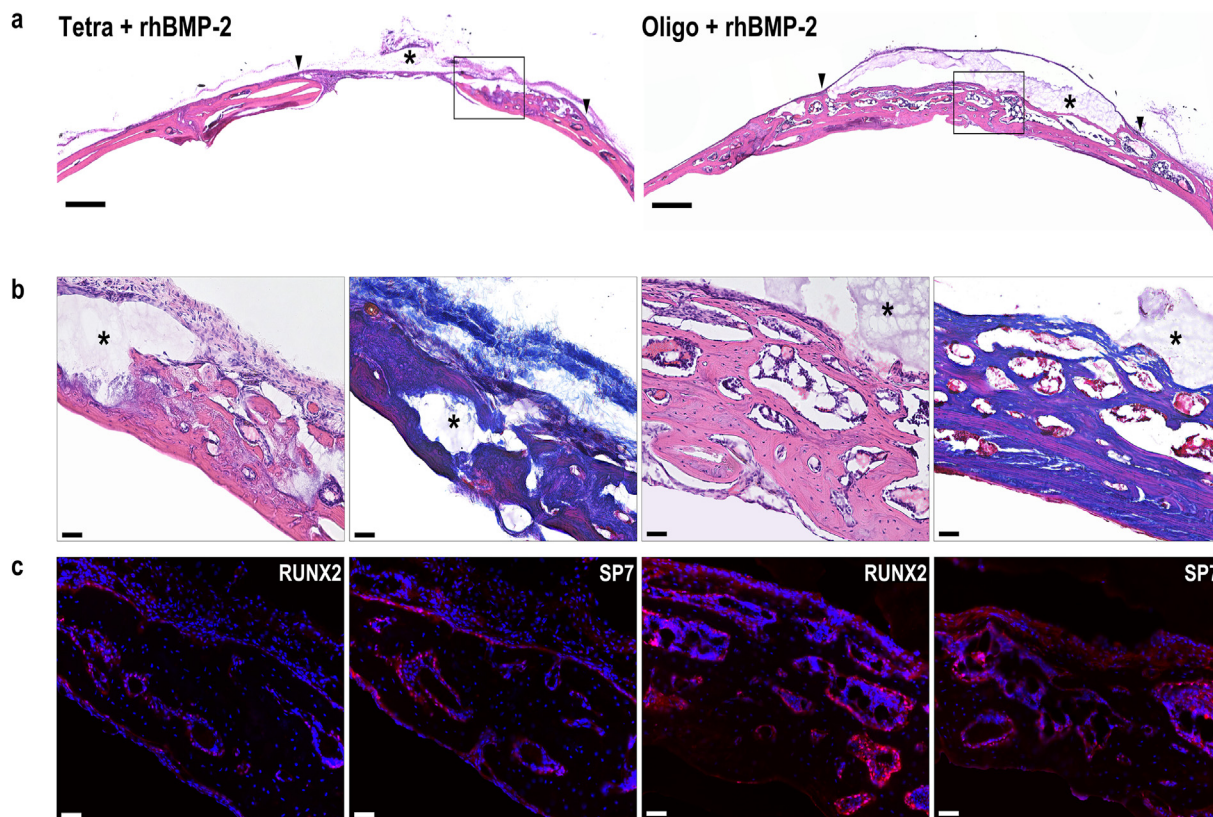


Fig. 5. Histological comparison of regenerated bone in mouse calvarial critical defects treated with rhBMP-2-loaded Tetra and Oligo gels at 42 days post-operation. (a) Whole view H&E staining of representative frozen sections of rhBMP-2-loaded Tetra and Oligo gel-treated defects. Arrowheads, asterisks, and rectangles denote the defect edges, hydrogel remnants, and the location of magnified images, respectively. Scale bars, 500 μm . (b) Magnified view of regenerated bone: H&E (left) and Masson's trichrome (right) staining. Scale bar, 50 μm . (c) Magnified view of regenerated bone: RUNX2 (left) and SP7 (right) immunostaining. Nuclei were stained with DAPI. Scale bars, 50 μm .

providing precise control of BMP signaling in a localized region [34]. Given the high affinity of BMPs for positive, negative, and hydrophobic surfaces, we hypothesized that the increased hydrophobicity of the Oligo gel would facilitate stronger protein-gel surface interactions when encapsulating rhBMP-2, allowing for its sustained release compared with Tetra gels [35–37]. Our findings from the analysis of protein release kinetics and osteoblast differentiation support this hypothesis.

Several research groups have investigated the potential of PEG-based hydrogels as scaffolds for localized and sustained release of rhBMP-2 for bone regeneration. Some of them have utilized PEG composite hydrogels, which involve copolymerizing PEG with other polymers such as poly (lactic-co-glycolic acid) (PLGA) or incorporating inorganic compounds such as collagen or hydroxyapatite [38–41]. PLGA is a hydrophobic polymer known for its biocompatibility and biodegradability, while collagen and hydroxyapatite possess osteoconductive properties [42–44]. Here, we briefly highlight relevant studies that have employed similar doses of rhBMP-2 and rodent calvarial defect models.

Rahman et al. developed a PEG hydrogel scaffold composited with PLGA and demonstrated the sustained release of rhBMP-2 over a 21-day period *in vitro*. When implanted *in vivo*, their scaffold loaded with 1 μg rhBMP-2 showed significant but incomplete regeneration of the defects in mice after 6 weeks. However, it is important to note that the defect size utilized in their study was a larger 4 mm-diameter defect [38].

Charles et al. grafted a PEG hydrogel scaffold with collagen and hydroxyapatite. Their study focused on the combinatorial effect of rhBMP-2 and recombinant human fibroblast growth factor-2 (rhFGF-2), an important growth factor for cell proliferation, in

regenerating 3.5 mm-diameter defects in young and old mice. Scaffolds loaded with 2 μg rhBMP-2, as well as a combination of 2 μg rhBMP-2 and 5 ng rhFGF-2, exhibited sustained release and achieved complete regeneration of defects in young mice after 4 weeks [39].

Seo et al. developed an injectable thermosensitive amphiphilic poly (phosphazene) nanoparticle composited with hydrophobic isoleucine ethyl ester and hydrophilic PEG. They demonstrated sustained release of rhBMP-2 over a 21-day period *in vitro*. However, in contrast with the aforementioned studies and our own, they opted to demonstrate orthotopic bone induction in mouse calvarias *in vivo*, showing significant bone generation, rather than utilizing a bone defect model [40].

Overall, compared to these studies, our work demonstrates that using an injectable hydrogel fabricated simply by reacting mutually reactive and highly branched tetra-armed PEG monomers could achieve comparable results in sustaining rhBMP-2 release and regenerating critical-sized defects to the more complex PEG composite scaffolds described above using similar doses of rhBMP-2. Our use of an extremely low polymer concentration in this study resulted in GGPS, which inherently provided key features such as hydrophobicity and porous structure to the hydrophilic bioinert Oligo gel. We believe that these features created a suitable environment within the bone defect for cells to migrate, proliferate, and differentiate.

There are several areas of focus for future research involving the Oligo gel that can advance our understanding and potential applications. Firstly, a comprehensive understanding of the mechanism of GGPS remains unclarified. The unanticipated observation of hydrophobicity in low concentration Tetra gels [15] and the even

greater hydrophobicity in Oligo gels demands further investigation. One possibility may be that despite the chemical components being the same in the two gels, the chemical structure is different. The Oligo pre-gel solutions are composed of highly branched polymeric clusters compared to the Tetra pre-gel solutions, which allows a more efficient network formation during gelation [14]. Therefore, as we previously suspected, gels may obtain unexpected physical properties depending on their chemical structures [15]. Additional studies are necessary to clarify the mechanism of GGPS.

Secondly, in our protein release kinetics studies, we solely examined at a loading concentration of 100 µg/ml. However, the release rate may vary with different loading concentrations. Future studies should encompass a range of concentrations to offer a more comprehensive view.

Thirdly, our histological analysis revealed the presence of residual gel in areas not overtaken by new bone. This indicates that the Oligo gel, in its current form, lacks the ability to self-degrade. To address this limitation, incorporating hydrolysable functionality in the gel might offer controlled degradation. In this case, finding a balance between controlled degradation and controlled release will be crucial to further improve the gel.

Fourthly, although our study demonstrated successful bone regeneration *in vivo*, there remains a gap in our knowledge regarding the mechanisms of molecular biology that govern the reactions and interactions between tetra-PEG gels and the bone defect microenvironment. To investigate cellular diversity inside the bone forming site, deeper analyses including single-cell RNA sequencing could be a valuable tool.

Finally, it is worth noting that the Oligo gel has previously been investigated as an artificial vitreous body to treat retinal detachment, highlighting its versatility and potential for various tissue engineering applications [14]. Owing to its easy formulation, injectability, and capacity for the sustained release of growth factors, the Oligo gel is a promising candidate biomaterial for a wide range of applications in regenerative medicine.

5. Conclusions

In this study, we demonstrated that oligo-tetra-PEG hydrogels undergo stronger gel-gel phase separation than their conventional tetra-PEG counterparts. This characteristic proved advantageous for retaining and sustaining the release of osteogenic growth factors to induce osteoblast cell differentiation over multiple sequential batches of cells and to enhance the repair of critical-sized bone defects *in vivo*. This biomaterial can be easily fabricated, which is beneficial for mass production. Its injectability and ability to sustain the release of growth factors make it a promising candidate biomaterial for a wide range of applications in regenerative medicine.

Author contributions

S.O. and H.H. conceived, designed, and supervised the project; T.S. designed Tetra and Oligo gels; S.N. designed and performed all experiments, including sample preparation, imaging, and data analysis with technical support from J.S. and suggestions from S.I.; M.N. and Y.S. supported experiments regarding SEM analysis; A.M.A. supported experiments regarding contact angles of gels; H.O. and U.C. contributed to discussions throughout the project; S.N. wrote the manuscript and S.I., H.O., S.O., U.C., T.S., and H.H. edited the manuscript.

Data availability

Data will be made available on request.

Declaration of competing interest

The authors declare that they have no known competing financial interests or personal relationships that could have appeared to influence the work reported in this paper.

Acknowledgements

We thank Dr. Shoichiro Tani at the University of Texas Southwestern Medical Center for providing technical assistance and insightful advice for our study; Dr. Shinse Fujita, Dr. Yoshiaki Kitaura, Akiko Nakamichi, Asuka Uchida, and Nozomi Nagumo at The University of Tokyo for providing technical assistance. This work was supported by Grants-in-Aid for Scientific Research from the Japan Society for the Promotion of Science (JSPS: 20H03885, 21H03142, and 21H04952), Rising Star Award from American Society for Bone and Mineral Research, the Japan Agency for Medical Research and Development (AMED; JP21bm0704071 and JP21zf0127002), and the Japan Science and Technology Agency (JST) FOREST Program (JPMJFR225N). This work utilized the core research facility of the Center for Disease Biology and Integrative Medicine at The University of Tokyo Graduate School of Medicine. S.N. and J.S. were supported by the Japanese Government (MEXT) and China Scholarship Council (CSC) scholarship programs, respectively.

Appendix A. Supplementary data

Supplementary data to this article can be found online at <https://doi.org/10.1016/j.reth.2023.11.008>.

References

- [1] Wu AM, et al. Global, regional, and national burden of bone fractures in 204 countries and territories, 1990–2019: a systematic analysis from the Global Burden of Disease Study 2019. *Lancet Healthy Longev* 2021;2(9). [https://doi.org/10.1016/S2666-7568\(21\)00172-0](https://doi.org/10.1016/S2666-7568(21)00172-0).
- [2] Salari N, et al. The global prevalence of osteoporosis in the world: a comprehensive systematic review and meta-analysis. *J Orthop Surg Res* 2021;16(1). <https://doi.org/10.1186/s13018-021-02772-0>.
- [3] Tessier P, et al. Autogenous bone grafts and bone substitutes - tools and techniques: I. A 20,000-case experience in maxillofacial and craniofacial surgery. *Plast Reconstr Surg* 2005;116(5 SUPPL). <https://doi.org/10.1097/01.prs.0000173862.20563.12>.
- [4] McDermott AM, et al. Recapitulating bone development for tissue regeneration through engineered mesenchymal condensations and mechanical cues. *Sci Transl Med* 2017;11:eaav7756. <https://doi.org/10.1101/157362>.
- [5] Maeda Y, et al. Bone healing by sterilizable calcium phosphate tetrapods eluting osteogenic molecules. *Biomaterials* 2013;34(22):5530–7. <https://doi.org/10.1016/j.biomaterials.2013.03.089>.
- [6] Agarwal R, Garcia AJ. Biomaterial strategies for engineering implants for enhanced osseointegration and bone repair. *Adv Drug Deliv Rev* 2015;94:53–62. <https://doi.org/10.1016/j.addr.2015.03.013>.
- [7] Alaribe FN, Manoto SL, Motaung SCKM. Scaffolds from biomaterials: advantages and limitations in bone and tissue engineering. *Biologia* 2016;71(4):353–66. <https://doi.org/10.1515/biolog-2016-0056>.
- [8] Bai X, Gao M, Syed S, Zhuang J, Xu X, Zhang XQ. Bioactive hydrogels for bone regeneration. *Bioact Mater* 2018;3(4):401–17. <https://doi.org/10.1016/j.bioactmat.2018.05.006>.
- [9] Li J, Mooney DJ. Designing hydrogels for controlled drug delivery. *Nat Rev Mater* 2016;1(12). <https://doi.org/10.1038/natrevmats.2016.71>.
- [10] Buwalda SJ, Vermonden T, Hennink WE. Hydrogels for therapeutic delivery: current developments and future directions. *Biomacromolecules* 2017;18:2. <https://doi.org/10.1021/acs.biomac.6b01604>.
- [11] Sakai T, et al. Design and fabrication of a high-strength hydrogel with ideally homogeneous network structure from tetrahedron-like macromonomers. *Macromolecules* 2008;41(14):5379–84. <https://doi.org/10.1021/ma800476x>.
- [12] Sugimura A, et al. Mechanical properties of a polymer network of Tetra-PEG gel. *Polym J* 2013;45(3):300–6. <https://doi.org/10.1038/pj.2012.149>.
- [13] Fuchs S, Shariati K, Ma M. Specialty tough hydrogels and their biomedical applications. *Adv Healthcare Mater* 2020;9(2). <https://doi.org/10.1002/adhm.201901396>.
- [14] Hayashi K, et al. Fast-forming hydrogel with ultralow polymeric content as an artificial vitreous body. *Nat Biomed Eng* 2017;1:44. <https://doi.org/10.1038/s41551-017-0044>.

- [15] Ishikawa S, et al. Percolation induced gel-gel phase separation in a dilute polymer network. *arXiv*; 2022. *preprint*, Feb.
- [16] Cross LM, Carrow JK, Ding X, Singh KA, Gaharwar AK. Sustained and prolonged delivery of protein therapeutics from two-dimensional nanosilicates. *ACS Appl Mater Interfaces* 2019;11(7). <https://doi.org/10.1021/acsami.8b17733>.
- [17] Delechiave G, et al. Tuning protein delivery from different architectures of layer-by-layer assemblies on polymer films. *Mater Adv* 2020;1(6). <https://doi.org/10.1039/d0ma00432d>.
- [18] Samsanraj RM, Dudakovic A, Zan P, Pichurin O, Cool SM, Van Wijnen AJ. A versatile protocol for studying calvarial bone defect healing in a mouse model. *Tissue Eng C Methods* 2017;23(11):686–93. <https://doi.org/10.1089/ten.tec.2017.0205>.
- [19] Shields LBE, et al. Adverse effects associated with high-dose recombinant human bone morphogenetic protein-2 use in anterior cervical spine fusion. *Spine (Phila Pa 2006)*;31(5). <https://doi.org/10.1097/01.brs.0000201424.27509.72>. 1976.
- [20] Hettiaratchi MH, Krishnan L, Rouse T, Chou C, McDevitt TC, Guldberg RE. Heparin-mediated delivery of bone morphogenetic protein-2 improves spatial localization of bone regeneration. *Sci Adv* 2020;6(1). <https://doi.org/10.1126/sciadv.aay1240>.
- [21] Boussein ML, Boyd SK, Christiansen BA, Guldberg RE, Jepsen KJ, Müller R. Guidelines for assessment of bone microstructure in rodents using micro-computed tomography. *J Bone Miner Res Jun*. 2010;25(7):1468–86. <https://doi.org/10.1002/jbmr.141>.
- [22] Roach P, Farrar D, Perry CC. Interpretation of protein adsorption: surface-induced conformational changes. *J Am Chem Soc* 2005;127:22. <https://doi.org/10.1021/ja042898o>.
- [23] Lommen J, et al. Release kinetics of the model protein FITC-BSA from different polymer-coated bovine bone substitutes. *Head Face Med* 2019;15(1). <https://doi.org/10.1186/s13005-019-0211-y>.
- [24] Wischke C, Borchert HH. Fluorescein isothiocyanate labelled bovine serum albumin (FITC-BSA) as a model protein drug: opportunities and drawbacks. *Pharmazie* 2006;61(9).
- [25] Kissling S, Seidenstuecker M, Pilz IH, Suedkamp NP, Mayr HO, Bernstein A. Sustained release of rhBMP-2 from microporous tricalciumphosphate using hydrogels as a carrier. *BMC Biotechnol* 2016;16(1). <https://doi.org/10.1186/s12896-016-0275-8>.
- [26] Li RH, Wozney JM. Delivering on the promise of bone morphogenetic proteins. *Trends Biotechnol* 2001;19(7). [https://doi.org/10.1016/S0167-7799\(01\)01665-1](https://doi.org/10.1016/S0167-7799(01)01665-1).
- [27] Capulli M, Paone R, Rucci N. Osteoblast and osteocyte: games without frontiers. *Arch Biochem Biophys* 2014;561. <https://doi.org/10.1016/j.abb.2014.05.003>.
- [28] Papageorgiou P, Vallmajo-Martin Q, Kisielow M, Sancho-Puchades A, Kleiner E, Ehrbar M. Expanded skeletal stem and progenitor cells promote and participate in induced bone regeneration at subcritical BMP-2 dose. *Biomaterials* 2019;217. <https://doi.org/10.1016/j.biomaterials.2019.119278>.
- [29] Aalami OO, et al. Applications of a mouse model of calvarial healing: differences in regenerative abilities of juveniles and adults. *Plast Reconstr Surg Sep*. 2004;114(3):713–20. <https://doi.org/10.1097/01.PRS.0000131016.12754.30>.
- [30] Cross M, Dexter TM. Growth factors in development, transformation, and tumorigenesis. *Cell* 1991;64(2). [https://doi.org/10.1016/0092-8674\(91\)90638-F](https://doi.org/10.1016/0092-8674(91)90638-F).
- [31] Kaspiris A, Hadjimichael AC, Vasiliadis ES, Papachristou DJ, Giannoudis PV, Panagiotopoulos EC. Therapeutic efficacy and safety of osteoinductive factors and cellular therapies for long bone fractures and non-unions: a meta-analysis and systematic review. *J Clin Med* 2022;11(13). <https://doi.org/10.3390/jcm11133901>.
- [32] Wegman F, Bijenhof A, Schuijff L, Öner FC, Dhert WJA, Alblas J. Osteogenic differentiation as a result of BMP-2 plasmid DNA based gene therapy in vitro and in vivo. *Eur Cell Mater* 2011;21. <https://doi.org/10.22203/eCM.v021a18>.
- [33] El Bialy I, Jiskoot W, Reza Nejadnik M. Formulation, delivery and stability of bone morphogenetic proteins for effective bone regeneration. *Pharmaceut Res* 2017;34(6). <https://doi.org/10.1007/s11095-017-2147-x>.
- [34] Lee K, Silva EA, Mooney DJ. Growth factor delivery-based tissue engineering: general approaches and a review of recent developments. *J R Soc Interface* 2011;8(55). <https://doi.org/10.1098/rsif.2010.0223>.
- [35] Utesch T, Daminelli G, Mroginski MA. Molecular dynamics simulations of the adsorption of bone morphogenetic protein-2 on surfaces with medical relevance. *Langmuir* 2011;27:21. <https://doi.org/10.1021/la202489w>.
- [36] Marquetti I, Desai S. Molecular modeling the adsorption behavior of bone morphogenetic protein-2 on hydrophobic and hydrophilic substrates. *Chem Phys Lett* 2018;706. <https://doi.org/10.1016/j.cplett.2018.06.015>.
- [37] Sundermann J, Zagst H, Kuntsche J, Wätzig H, Bunjes H. Bone morphogenetic protein 2 (BMP-2) aggregates can be solubilized by albumin—investigation of BMP-2 aggregation by light scattering and electrophoresis. *Pharmaceutics* 2020;12(12). <https://doi.org/10.3390/pharmaceutics12121143>.
- [38] Rahman CV, et al. Controlled release of BMP-2 from a sintered polymer scaffold enhances bone repair in a mouse calvarial defect model. *J Tissue Eng Regen Med* 2014;8(1). <https://doi.org/10.1002/term.1497>.
- [39] Charles LF, Woodman JL, Ueno D, Gronowicz G, Hurley MM, Kuhn LT. Effects of low dose FGF-2 and BMP-2 on healing of calvarial defects in old mice. *Exp Gerontol* 2015;64. <https://doi.org/10.1016/j.exger.2015.02.006>.
- [40] Seo B-B, Choi H, Koh J-T, Song S-C. Sustained BMP-2 delivery and injectable bone regeneration using thermosensitive polymeric nanoparticle hydrogel bearing dual interactions with BMP-2. *J Contr Release Jul*. 2015;209:67–76. <https://doi.org/10.1016/j.jconrel.2015.04.023>.
- [41] Sun S, et al. Drug delivery systems based on polyethylene glycol hydrogels for enhanced bone regeneration. *Front Bioeng Biotechnol* 2023;11. <https://doi.org/10.3389/fbioe.2023.1117647>.
- [42] Makadia HK, Siegel SJ. Poly Lactic-co-Glycolic Acid (PLGA) as biodegradable controlled drug delivery carrier. *Polymers* 2011;3:3. <https://doi.org/10.3390/polym3031377>.
- [43] Gentile P, Chiono V, Carmagnola I, Hatton PV. An overview of poly(lactic-co-glycolic) Acid (PLGA)-based biomaterials for bone tissue engineering. *Int J Mol Sci* 2014;15(3). <https://doi.org/10.3390/ijms15033640>.
- [44] Wahl DA, Czernuszka JT. Collagen-hydroxyapatite composites for hard tissue repair. *Eur Cell Mater* 2006;11. <https://doi.org/10.22203/eCM.v011a06>.